Direct numerical simulation of a particle-laden weak-shearing plane jet*

XIA Jun[1**], HU Guilin[2], FAN Jianren[2] and CEN Kefa[2]

(1. College of Computer Science, and Center for Engineering and Scientific Computation, Zhejiang University, Hangzhou 310027, China; 2. Institute for Thermal Power Engineering, College of Mechanical and Energy Engineering, Zhejiang University, Hangzhou 310027, China)

Received June 27, 2003; revised August 25, 2003

Abstract Direct numerical simulation (DNS) has been utilized to solve numerically a two-dimensional compressible weak-shearing plane jet, in which the jet exit velocity and the co-flow velocity are in the same magnitude (2∶1 in this paper). We also use the one-way coupling method to simulate the dispersion behaviors of solid particles in various representative sizes, i.e. St=0.01, 1, 10, 100, where St is the Stokes number. We get a vorticity field with fully varicose (symmetrical) modes and the entire precise processes of the rolling-up of one spanwise vortex, the pairing of two vortexes and the mixing of three vortexes. The mean longitudinal velocity (U) profile compares well against the experimental results. The Reynolds stress profile looks special due to the symmetrical vorticity field. The particles whose St=0.01 reproduce the vortex structures in detail, and the ones of St=1 exhibit interesting self-organized behaviors and possess the most non-uniform concentration field. They disperse uniformly around the single and pairing vortex kernels, while a few of them are arranged almost in a straight line in the center region of the paring vortexes, which is caused by the contribution of the border of two vortexes in the pairing process. St=10 and 100 can be treated as large particles, on which the flow field has few impacts.

Keywords: direct numerical simulation (DNS), plane turbulent jets, vortex structures, solid particles, Stokes number.

The free shear flow is a classical flow phenomenon containing transition and turbulence, and the plane jet is a sort of free shear flow whose structures are more complicated than those of plane mixing layers. Up to now, many studies concentrate on round and rectangular jets, however, the plane jets, which are also a prototypical sort of free turbulent shear flow in a broad number of engineering applications, have been somewhat ignored. To the best of our knowledge, this paper is a rather early conducted research on direct numerical simulation (DNS) of gas-solid two-phase plane turbulent jets in domestic research work of computational fluid dynamics (CFD).

In early experimental work of plane turbulent jets, Bradbury[1] and Everitt et al.[2] found that the presence of strong co-flows will slow the progress of the jet to a self-similar state. Everitt et al.[2] studied the flow structure and evolution of turbulent plane jets in both stagnant and moving stream. The measuring results showed that the large scale structures did not exist in the jet in quiescent co-flow, which can be found obviously in the jet in moving streams and described by "local flapping". The early work of Sato[3] and Rockwell et al.[4] showed that the varicose mode, i.e. the flow structures predominately being symmetrical, is most commonly observed in the nearfield of planar jets. The asymmetric or sinuous mode in the jet was the characteristic of curved mean velocity profile. So, if we arrange the exit velocity in curved profile, the asymmetric mode can be observed downstream near the jet nozzle. Generally, the transition from the symmetric frame near the jet nozzle to the asymmetric configuration in the fully developed region was found to take place after the mixing of the two shear layers, but before the start location of similarity[5], in which the mean velocity profile transfers from a flat profile to a curved one.

Compared with experimental studies, numerical studies of planar jets are much fewer. The earliest numerical work was conducted by Oler et al.[6]. They performed preliminary jet simulations by treating the fully developed region of the jet as a spatially evolving vortex street composed of overlapping Rankine vortices. Dai et al.[7] first performed large eddy simulation of a spatially evolving subsonic planar jet. They got satisfied mean profiles which compared well with experimental results, but the fluctuation intensities were 40% higher. Reichert et al.[8] studied how

* Supported by the National Natural Science Foundation of China (Grant No. 50236030)

** To whom correspondence should be addressed. E-mail: jxia@zju.edu.cn

the compressibility influences the spatially evolving flow structures in a 2-dimensional inviscid jet with strong co-flow stream. They found that the jet growth rate and entrainment decrease as the convective Mach number, M_c, grows. When $M_c = 0.4$, the entrainment completely disappears in the self-similar region. Though quite a few numerical studies have been focused on rectangular[9, 10] and round[11, 12] jets, there is considerably less relevant research on planar jets.

There have been few two-phase flow simulations with advanced numerical methods (DNS/LES). In all the simulation work of particle dispersion with one-way coupling in the free shear layers, discrete vortex simulations have played an important role, which works well in the simulations of temporal and spatially evolving plane mixing layers[13, 14], spatial axisymmetric jets[15] and spatial plane wakes[16]. However, all these simulations require two-dimensional and inviscid hypotheses. Generally, the existence of particles will influence the large scale turbulent structures. For example, in the two-dimensional simulations of free shear layers, Tang et al.[17] found that particles slow the pairing mechanisms. Fan et al.[18] used DNS to study the dispersion characteristic of various particles in a temporal mixing layer. Jin[1)] performed large eddy simulations of gas-solid two phase jets and studied the particle dispersion rules in the jet field with both one-way and two-way coupling methods. His results indicated that the existence of particles will generally retard the development of turbulent coherent structures, while promoting the evolution instead if the mass loading rate is a little higher. But so far, the authors have found considerably fewer two-phase jet simulations with DNS, especially in China. This paper presents direct numerical simulations, which is based on finite difference methods, of one-way coupling particle-laden weak-shearing jets.

1 Governing equations

1.1 Equations of the flow field

This paper studies the compressible ideal gas. We assume that the fluid properties are constant in time and space, and that the influence of the gravity is omitted. The governing equations include the continuous equation, N-S equations and the energy equation, which is expressed in pressure p, as shown respectively in the following:

$$\frac{\partial \rho}{\partial t} + \frac{\partial(\rho u_k)}{\partial x_k} = 0, \tag{1}$$

$$\frac{\partial(\rho u_i)}{\partial t} + \frac{\partial(\rho u_i u_k)}{\partial x_k} = -\frac{\partial p}{\partial x_i} + \frac{1}{Re}\frac{\partial \tau_{ij}}{\partial x_j}, \tag{2}$$

where the viscous stress tensor

$$\tau_{ij} = \mu\left(\frac{\partial u_i}{\partial x_j} + \frac{\partial u_j}{\partial x_i}\right) - \frac{2}{3}\mu\frac{\partial u_k}{\partial x_k}\delta_{ij}, \tag{3}$$

$$\frac{\partial p}{\partial t} + u_k\frac{\partial p}{\partial x_k} + \gamma p\frac{\partial u_k}{\partial x_k} = \frac{\gamma}{PrRe}\frac{\partial}{\partial x_k}\left(\kappa\frac{\partial T}{\partial x_k}\right) + \frac{\gamma - 1}{Re}\phi, \tag{4}$$

in which the viscous dissipation

$$\phi = \tau_{ij}\frac{\partial u_i}{\partial x_j}. \tag{5}$$

The state equation of the ideal gas,

$$p = \rho R T \tag{6}$$

is also needed, through which the pressure p and temperature T are related. All the above equations have been normalized.

1.2 The equation of the particle motion

This paper focuses on the dispersion characteristic of the solid particles in the jet field. The following assumptions have been made:

(i) The particle system is treated as a dilute phase, i.e. we have not considered the mutual collisions between particles.

(ii) All the particles entering the computational domain are in regular spherical shapes, and their diameters, d_p, and densities, ρ_p, are constant.

(iii) The density of particles is much bigger than that of the gas.

(iv) We consider only the drag force of the flow field and the gravitational force of particles themselves on particles when they stay in the computational domain.

Then, the normalized vector motion equation of particles is written as

$$\frac{\mathrm{d}\boldsymbol{V}}{\mathrm{d}t} = \frac{f}{St}(\boldsymbol{U} - \boldsymbol{V}) + \boldsymbol{g}, \tag{7}$$

where f is the modified factor of the drag force coeffi-

1) Jin, H. H. Large eddy simulation of coherent structure in gas-particle two phase turbulence. Ph. D. Dissertation, Zhejiang University, 2002.

cient, $f = 1 + 0.15Re_p^{0.687}$ [1]. Re_p is the particle Reynolds number, $Re_p = |\boldsymbol{U} - \boldsymbol{V}| d_p/\nu$. St is the Stokes number, $St = \dfrac{\rho_p d_p^2/(18\mu)}{l_r/u_r}$. $\boldsymbol{U}$ and $\boldsymbol{V}$ are the velocity vectors of the gas and particle phase, respectively. $\boldsymbol{g}$ is the gravitational acceleration vector.

Integrating (7), we get the velocity and position vectors of every particle,

$$\boldsymbol{V}^{n+1} = \boldsymbol{U} + \frac{St}{f}\boldsymbol{g} + \left(\boldsymbol{V}^n - \boldsymbol{U} - \frac{St}{f}\boldsymbol{g}\right) \cdot \exp(-f\Delta t/St), \tag{8}$$

$$\boldsymbol{x}_p^{n+1} = \boldsymbol{x}_p^n + \boldsymbol{U}\Delta t + \frac{St}{f}\boldsymbol{g}\Delta t + \frac{St}{f}\left(\boldsymbol{V}^n - \boldsymbol{U} - \frac{St}{f}\boldsymbol{g}\right) \cdot [1 - \exp(-f\Delta t/St)], \tag{9}$$

where n, $n+1$ represent the present and next time step, respectively.

2 Numerical methods

Compact finite difference schemes have been used in space discretization. The 1st-derivative and 2nd-derivative terms are discretized by 4th-order central difference schemes, both of which are tri-diagonal and have 3-4-3 precision frames[19]. The cross derivative terms $\partial^2 V/\partial x\partial y$ are evaluated by consecutively solving the 1st-derivative twice. Because the compact scheme will produce the maximal errors at the highest wave number supported by the computational grids, filtering the numerical results is necessary, which is done by a 4th-order compact filter herein.

We utilize different integration schemes to treat Euler terms and non-Euler terms, the former of which is marched in time by low-storage 4th-order explicit Runge-Kutta schemes[20], while the latter of which by 1st-order explicit Euler scheme, which can save computational time considerably. We can dispose in this way because the coefficients of every non-Euler term, including the viscous and conduction one, contain an item of $1/Re$, which causes the magnitude of the whole term to be very small due to the large jet Reynolds number ($Re \approx 7000$ herein) compared with that of Euler terms. This technique has been effectively used in predecessors' numerical simulations[2].

One of the most difficult factors in DNS of free jets lies in the setting of boundary conditions. Generally, the jet flow develops in an infinite or very large domain, but we must truncate the open space into a finite domain to carry out the computations, which brings out the problems, i.e. we do not know the field information outside the computational domain which crosses the boundary into the computational domain. Non-reflecting boundary conditions (NRBCs)[21, 22] have been employed in this paper to minimize this effect, which also minimize the numerical reflected waves back into the computational domain at the boundary which do not exist physically. It can be described simply as follows: at the individual point at the boundary, if the direction of the normal velocity is outgoing, compute the normal derivatives of all flow variables as usual, whereas set the derivative values to zero. At the outflow boundary, because all the large scale structures propagate almost in the normal direction of the boundary, Thompson's NRBCs based on one-dimensional system are capable of letting the vortexes pass through the boundary fluently. However, the perfectly NRBCs may lead to pathological numerical solutions, so the pressure correction terms proposed by Rudy et al.[23] are adopted at the outflow boundary simultaneously.

At the inflow boundary, we set the density and mean velocity profiles in advance, so NRBCs are not fit any more apparently. The characteristic inflow boundary conditions (CIBCs)[24] are used to evaluate the time variation of pressure p. In order to speculate the time variation of the amplitudes of characteristic waves, CIBCs transform the multi-dimensional viscous problem to a one-dimensional inviscid one, which was called the local one-dimensional inviscid (LODI) relations by Poinsot et al.[24]

At the two far-field boundaries, the authors found that even a stochastic numerical error can easily aggregate gradually in the interior domain and contaminate the flow field finally, so NRBCs may not be good enough in this situation. We used perfectly matched layer (PML) buffer zone techniques[25, 26], which append another nonphysical region at the end of the original computational domain and a damping term in every governing equation to damp all the dependant variables to the known mean states. Because the damping coefficient σ has been set to a very large number (100) herein, we discarded NRBCs at the

1) Zheng, Y. Q. Direct numerical simulation and experimental verification on the turbulent coherent structures in gas-particle two-phase mixing layer. Ph. D. Dissertation, Zhejiang University, 2001.

2) Stanley, A. S. A computational study of spatially evolving turbulent plane jets. Ph. D. Dissertation, University of California, San Diego, 1998.

far-field boundaries (see footnote on this page for reference).

In the integrated N-S equations, viscous boundary conditions are also required. The recommended schemes of Poinsot et al.[24] have been utilized in this paper, i.e. in x direction, for example, $\partial\tau_{xy}/\partial x = \partial q_x/\partial x = 0$ for an outflow boundary, at which the normal velocity direction is coincident with the outward normal direction of the boundary, and $\partial\tau_{xx}/\partial x = 0$ for an inflow boundary.

At the inflow boundary, the longitudinal velocity profiles of either shear layer of the jet, which are symmetrical with the jet centerline, are set to the familiar hyperbolic tangent curves,

$$u = \frac{U_1 + U_2}{2} + \frac{U_1 - U_2}{2}\tanh\left(\frac{y}{2\theta}\right), \quad (10)$$

and all the lateral velocities (V) are set to zero. We arrange the same velocity profiles in the whole computational domain as those at the inflow initially.

As we track particles in the jet flow field, the density and velocity values should be used after interpolated, for it is not general for particles to just stay on the grid points at any time. The bilinear interpolation scheme has been used in this paper. It should be pointed out that the one-way coupling method has been utilized herein to track particles, so the precision order of numerical results of the particle phase has no influence on that of the gas phase. In addition, the preliminary statistical results of the particle phase have been precise enough, so it is appropriate to use first-order bilinear interpolation to satisfy the precision requirement. It should be necessary to utilize higher-order Lagrangian or Hermite interpolation schemes in two-way coupling methods.

3 Results and discussions

We take the air in ordinary conditions as the simulation gas, i.e. the environmental pressure and temperature are 101.325 kPa and 20°, respectively. The velocity ratio $\eta = \Delta U/(U_1 - U_2) \approx 0.33$. The jet Reynolds number $Re_h = \rho\Delta U h/\mu \approx 7056$. The ratio of initial momentum thickness to jet slot width $\theta/h = 0.025$, so in terms of shear layer parameters, the Reynolds number based on momentum thickness $Re_\theta = \rho\Delta U\theta/\mu \approx 176$. The convective Mach number $M_c = \Delta U/(c_1 + c_2) \approx 0.125$.

The computational domain size is set to $L_x = 15h$ and $L_y \approx 5.9h$. In y direction, physical section lasts $5h$, while the residual $0.9h$ is assigned averagely at both ends of physical domain as PML buffer zones. We choose a computing grid system $375 \times (11 + 229 + 11)$, where 11 is the grid point numbers in buffer zones. The grid is uniform in x direction, $\Delta x \approx 0.04h$, while in y direction, we arrange uniform grids in the physical domain, $\Delta y \approx 0.022h$, and stretched grids in buffer zones, where the stretching ratio is 10%.

Fig. 1 is the vorticity contour plots in the weak-shearing jet, where t_c is the convective flow time, $t_c = L_x/U_c$, U_c is the average velocity at the jet slot, $U_c = (U_1 + U_2)/2$. It can be found that due to the existence of strong co-flow stream, no obvious interaction between the two free shear layers near the slot has occurred so that the development of vortex structures is similar to what appeared in the spatially evolving mixing layers. Two von Karman-like vortex streets with opposite sign appear. In (a), in the section $x/h = 2.5 \sim 3$, the waves whose frequencies correspond to the natural frequencies are enlarged to the saturated state, so the spanwise vortexes roll up and march downstream with the convective velocity U_c. With the increase of Reynolds number, this kind of periodic flow structure will lose its stability again which leads to vortex pairing and mixing. $t = 3t_c$ is a special instantaneous while, when no vortex pairing appears and all the single spanwise vortexes arrange regularly in the computational domain. The number of vortexes attains a maximal value -10 in both the upper and lower vortex streets. If the forces with the fundamental and first subharmonic frequencies are imported at the inflow boundary, (b) may be compelled to a stable vortex structure frame, i.e. the pairing of spanwise vortexes is inhibited, which is interesting and profound in the research of vortex control. When $t = 3.5t_c$, the flow has developed to a mean stable state. The downstream position of the rolling-up of spanwise vortexes is generally fixed, about at $x/h = 2.5 \sim 3$. In the computational domain, the number of times of vortex pairing is generally bigger than 2. We have also captured the phenomenon of 3 vortex mixing. For example, in (c), the vortex structure near the outflow boundary comes into being after 3 vortex mixing. The flow structures at both sides of the jet centerline almost keep sym-

1) Xia, J. Direct numerical simulation of gas-solid two-phase plane turbulent jets. Ph. D. Dissertation, Zhejiang University, 2002.

metrical at all time.

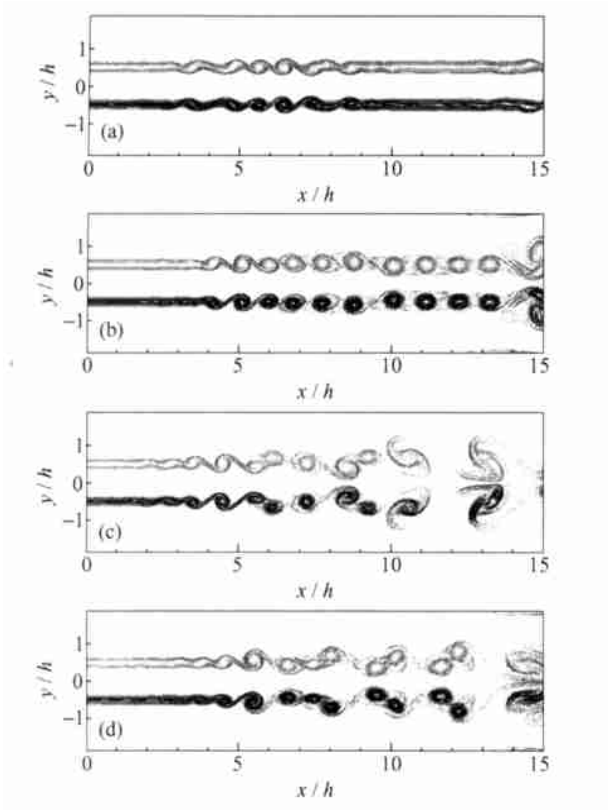

Fig. 1. The vorticity fields in the weak-shearing jet. (a) $t=2t_c$; (b) $t=3t_c$; (c) $t=4t_c$; (d) $t=5t_c$.

Fig. 2(a) is the vorticity contour plot of one spanwise rolled-up vortex kernel, and (b) is the topology structure of one vortex by theoretical analysis. It can be found that their description about a single vortex is completely coherent. In our results, during the rolling-up process, the marching velocity of the flow structures $U_r=1.5=U_c$, equal to the convective velocity. The whole process is finished in the section of $x/h=2.5\sim7.1$. After full rolling-up, the vortex kernel possesses an elliptical shape whose size is $0.6h\times0.5h$. The vortex core always holds at $y/h=0.5$, where the strongest shearing effects emerge.

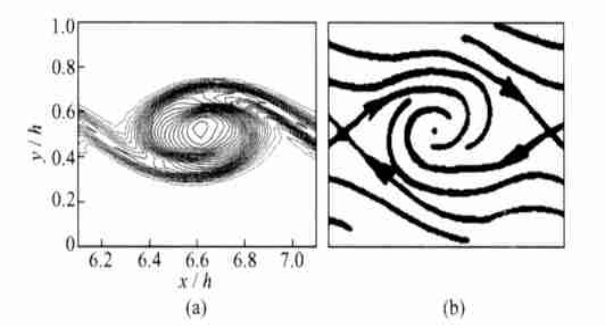

Fig. 2. One spanwise vortex. (a) Computational results; (b) topology structure from Tong et al.[27]

Fig. 3 shows the representative vorticity contour plot during the pairing process and the predecessor's relevant results, which are fairly similar at qualitative level. Similar to the situation when vortexes roll up, the marching velocity of pairing vortexes is approximately equal to the convective velocity U_c. In the whole period of pairing, the biggest lateral size of vortex kernels extends about $1h\sim1.1h$, which is two times the lateral width ($0.5h$) of a single spanwise vortex after the rolling-up finishes. So, from the end of the rolling-up of spanwise vortexes to the end of the pairing of two vortexes, both the size scale of vortexes and shear-layer thickness double.

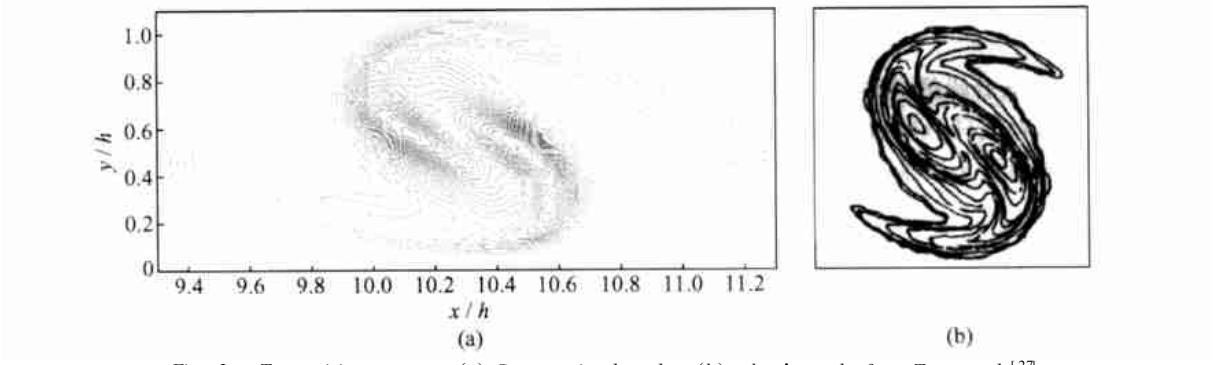

Fig. 3. Two pairing vortexes. (a) Computational results; (b) others' results from Tong et al.[27]

The computational results have captured the complete process of 3-vortex mixing, as shown in Fig. 4. If just judging from the phenomenon, the 3-vortex mixing can be linearly divided into two consecutive 2-vortex pairing. During the process of 3-vortex mixing, the marching velocity of large scale structures is about 1.56, a little bigger than the convective velocity U_c. The biggest lateral extending range of the vortexes ($1.3h$) is a bit smaller than 3 times of the width in y direction of a single vortex kernel. It

should be pointed out that the simulation object in this paper is a free jet flow developing in symmetrical modes, so on the other side of the jet centerline, there exist the vortex structures with the same figures and opposite signs so that the vorticities on either side of the centerline must squash each other and cannot develop without limit. In this sense, we can make the conclusion that as 3 vortexes mix, the biggest lateral size scale is 3 times that of one rolling-up vortex.

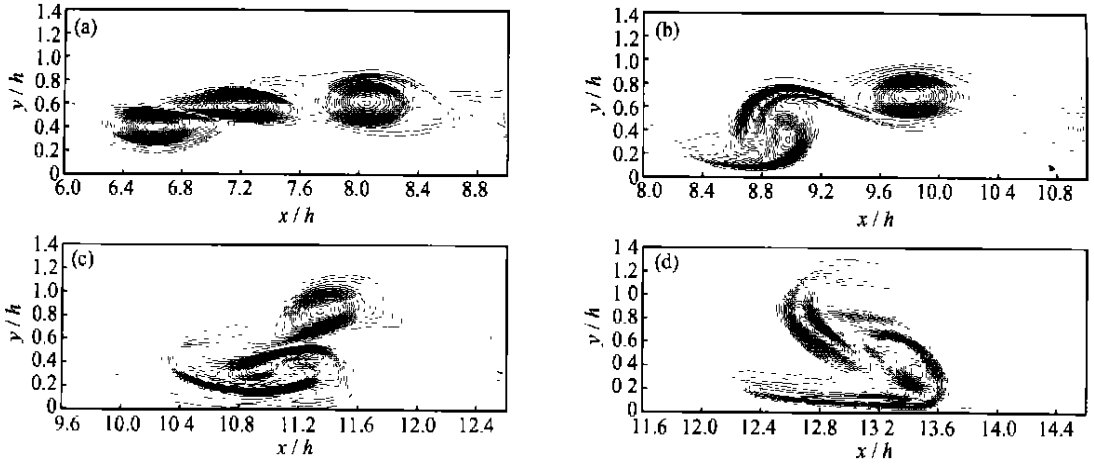

Fig. 4. Three vortexes' mixing.

Fig. 5 is the mean longitudinal velocity (U) profile in the weak-shearing plane jet, where δ_U is the local jet half width. The experimental results measured under similar conditions[11] are also given. We can see that U does not get to the self-similar state until $x/h=11.5$. Fig. 5 shows the U profiles at 5 stations, i.e. $x/h=11.5$, 12, 13, 14, 14.5, which almost overlap in one parabolic line. Furthermore, the computational results coincide with the experimental ones, which proves even if the DNS results are got in 2-dimensional cases, they can reproduce precisely enough the mean velocity profiles of "real" flows, and that the streamwise flow structures have few effects on the U profile.

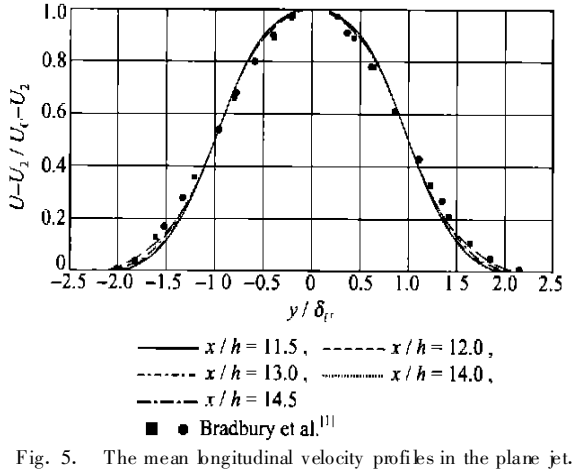

Fig. 5. The mean longitudinal velocity profiles in the plane jet.

Fig. 6 gives the longitudinal and lateral fluctuation velocity profiles, which exhibit typical fluctuation characteristic of jets developing in symmetrical modes. This kind of symmetry has remarkably influenced the development of fluctuation fields. The lateral Reynolds stresses at the jet centerline $\sqrt{\overline{v_C^2}}$ are inhibited. At the same time, the longitudinal centerline stresses $\sqrt{\overline{u_C^2}}$ tend to grow continuously, and as a result at the downstream station $x/h=10$, $\sqrt{\overline{u_C^2}}$ have grown to a value almost equal to the peak stresses at the center of shear layers. Obviously, this is a special instance in the 2-dimensional jets which possess symmetrical vortex streets. The fluctuation parameters have not got to the self-similar state yet in the computational domain ($x/h=0\sim15$). The experimental results[28] showed that in the jet flow system with low speed co-flow stream, the self-similar profile will not appear until the downstream streamwise displacement has got across $30h$. In this paper, the existence of strong co-flow ($U_1:U_2=2:1$) further delays the process of Reynolds stresses developing to the self-similar states.

Various particles in 4 prototypical sizes, i.e. $St=0.01$, 1, 10, 100, have been studied in this paper. We hope our computational results can provide helpful references for engineering practice, such as optimizing the particle size to improve the combustion efficiency in burner systems.

Particles enter the computational domain after one convective flow cycle in all cases. The entrance

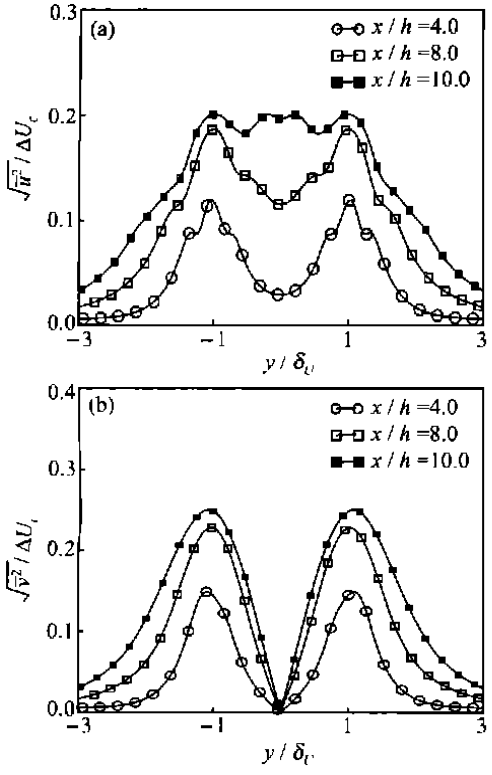

Fig. 6. The fluctuation velocity profiles in the plane jet. (a) Longitudinal components; (b) lateral components.

numbers at the jet nozzle of all the above particles are set to 151, 151, 151 and 57, respectively. We use the data structure of "List" to record the particle information to save the memory consumption.

Fig. 7 is the instantaneous dispersion fields of various particles at $t=4t_c$. The corresponding vorticity field is Fig. 1(c). The particle numbers in the computational domain in Fig. 7 are 41925, 39950, 38171 and 14294, respectively. We can see that as $St \ll 1$, the particle distribution is fully controlled by the jet shear layers. During the rolling-up of spanwise vortexes, these particles gradually move helically from the outside of the kernel into the core as the vortex forms. Particles in similar sizes can be treated as "tracking" ones, i.e. reproducing the complete process of the development of vortex structures in jet shear layers. In the following vortex-pairing stage, particles arranging orderly in the two vortexes mix with each other and the arrangement develops towards non-orderly manner. We get very interesting results similar to those of predecessors as $St \sim O(1)$. In this case, the dynamic response time of particles, τ_R, and the characteristic time of the fluid flow, τ_F, are in the same magnitude, which causes almost all the particles to aggregate outside the single spanwise vortex kernel and at the border of two vortexes in the pairing process, i.e. the particle dispersion field is most non-uniform. With the augment of particle sizes, their inertia gradually strengthens and these particles cannot be easily involved by the large scale structures. As $St=10$, particles sweep little in the domain where vortexes exist, but cannot propagate through the whole vortex any longer. As $St=100$, almost all the particles stay in the band section whose width is equal to h. At the center sections of two jet shear layers in the computational domain ($y=\pm 0.5h$), the particle concentration is higher. It should be pointed out that for all these various particles of 4 classes, the maximal particle numbers in one computational grid, $n_{i\max}=11(St=0.01)$, 36(1), 11(10) and 3(100), respectively, have been got in the shear layer sections. We can also see hereinabove that as $St \sim O(1)$, the particle distribution is most non-uniform, i.e. most particles assembling in LOCAL domains.

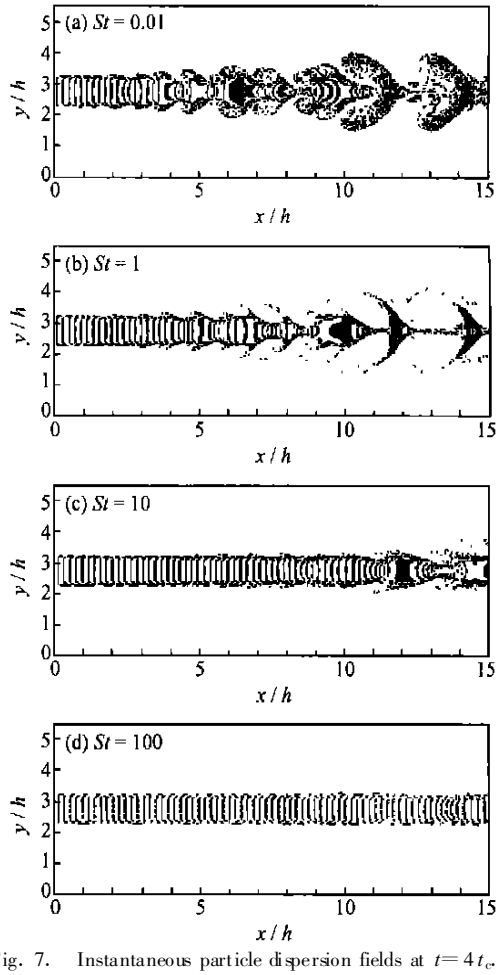

Fig. 7. Instantaneous particle dispersion fields at $t=4t_c$.

In order to describe the characteristic of the particle concentration field and the detailed extent of the

particle dispersion, we introduce the grid RMS particle numbers, N_{rms}, which is defined as

$$N_{rms} = \left(\sum_{i=1}^{n_t} n_i^2 / n_t \right)^{1/2}, \quad (11)$$

where n_t is the total grids in the computational domain, i.e. the number of collocation grid points, $n_t = 374 \times 228 = 85272$; n_i is the particle number in the ith grid at some instantaneous while. When $t = 0$, $N_{rms} = 0$ if we follow the above definition.

Table 1 is the N_{rms} values of particles at various Stokes numbers at 4 instantaneous whiles. We can see that $N_{rms}(St = 1)$ is always the biggest at different time, which proves particles in similar sizes possess the most non-uniform concentration field and the biggest dispersion scope in the flow field. The large scale structures influence the particle dispersion most strongly as the magnitude of the dynamic response time of particles is similar to that of the characteristic time of the fluid flow. On the other hand, N_{rms} values are relatively small with regard to particles at other Stokes numbers, i.e. the dispersion fields are more uniform. If comparing $N_{rms}(St = 0.01)$ with N_{rms} $(St = 10)$, we can find that their difference is very small (about 0.01 ~ 0.02 in the magnitude). Additionally, their n_{imax} values are completely the same (11). All of these indicate that there exist similarities between particles of $St = 0.01$ and those of 10 in some statistical results, like N_{rms}, and microcosmic characters, like n_{imax}, even if their dispersion behaviors seem entirely different in the weak-shearing jet flow field. Further studies will be needed in relevant subjects.

Table 1. N_{rms} values of particles of 4 representative classes

N_{rms}	St			
	0.01	1	10	100
$3.5t_c$	1.3721	1.5992	1.3923	0.5528
$4t_c$	1.3848	1.7211	1.3904	0.5543
$4.5t_c$	1.4100	1.6716	1.3912	0.5544
$5t_c$	1.3820	1.5988	1.3960	0.5543

The velocity field V_r of particles relative to the gas phase can show directly the moving tendency of particles in the flow field at any time, so it is a good quantitative means to study the dispersion characteristic of particles. Fig. 8 is the relative velocity vector fields V_r of all the studied particles at one typical while during the pairing of two vortexes. The corresponding vorticity contour field is Fig. 3(a). Because the inertia of small particles ($St = 0.01$) is weak, we can see that almost all their relative velocities are zero. These particles can follow the vorticity contour lines from the outside into the interior of the vortex and reflect the coherent structures equivalently at that time. Consequently, very small particles are usually used as "tracking" ones in experiments to reproduce the instantaneous flow structures. As $St = 1$, almost all the particles disperse outside the vortex kernel and the directions of V_r are all leaving the vortexes, which indicates that they are willing to spread out further. A few of them arrange orderly almost in a line in the vortexes. They are controlled by the "folding" effects at the border of two vortexes in pairing. It can be found that the line formed by the particles lags behind the real vortex border, for the movement of vortexes directs that of particles. The cross angle is about 90° in this paper. Furthermore, at both sides of the line, the magnitudes of relative velocities of particles are almost the same, but their directions are opposite, which shows that the rotating directions of the two vortexes in pairing are fully contrary. As to the large particles of $St = 10$ and 100, they are capable of sustaining their own moving tendency. Because of the large inertia, they are less influenced by the large scale structures.

To sum up from the above discussions, we think that the small particle in "tracking" magnitudes is the optimal choice to improve the combustion efficiency. If we treat the jet flow in this paper as a burner system in engineering applications, i.e. the jet nozzle is the primary air exit and the region where the co-flow stream occupies is the overfire air port—the most popular arrangement of annular burners, the contact surface area between particles of $St = 0.01$ and air is the biggest in all cases judging from Figs. 7, 8 and Table 1, so they mix most intensively and the abundant combustion will take place most probably.

4 Conclusions

The greatest difficulties in DNS of external, spatially evolving flows, such as the free jet in this paper, lie in the setting of boundary conditions. The detailed flow structures explored by the computational results prove the validity of BCs adopted in this paper.

Two fully symmetrical vortex streets develop at the downstream section of the jet nozzle in the computational domain, in which the rolling-up of one spanwise vortex, the pairing of 2 vortexes and the mixing of 3 vortexes take place. During both the

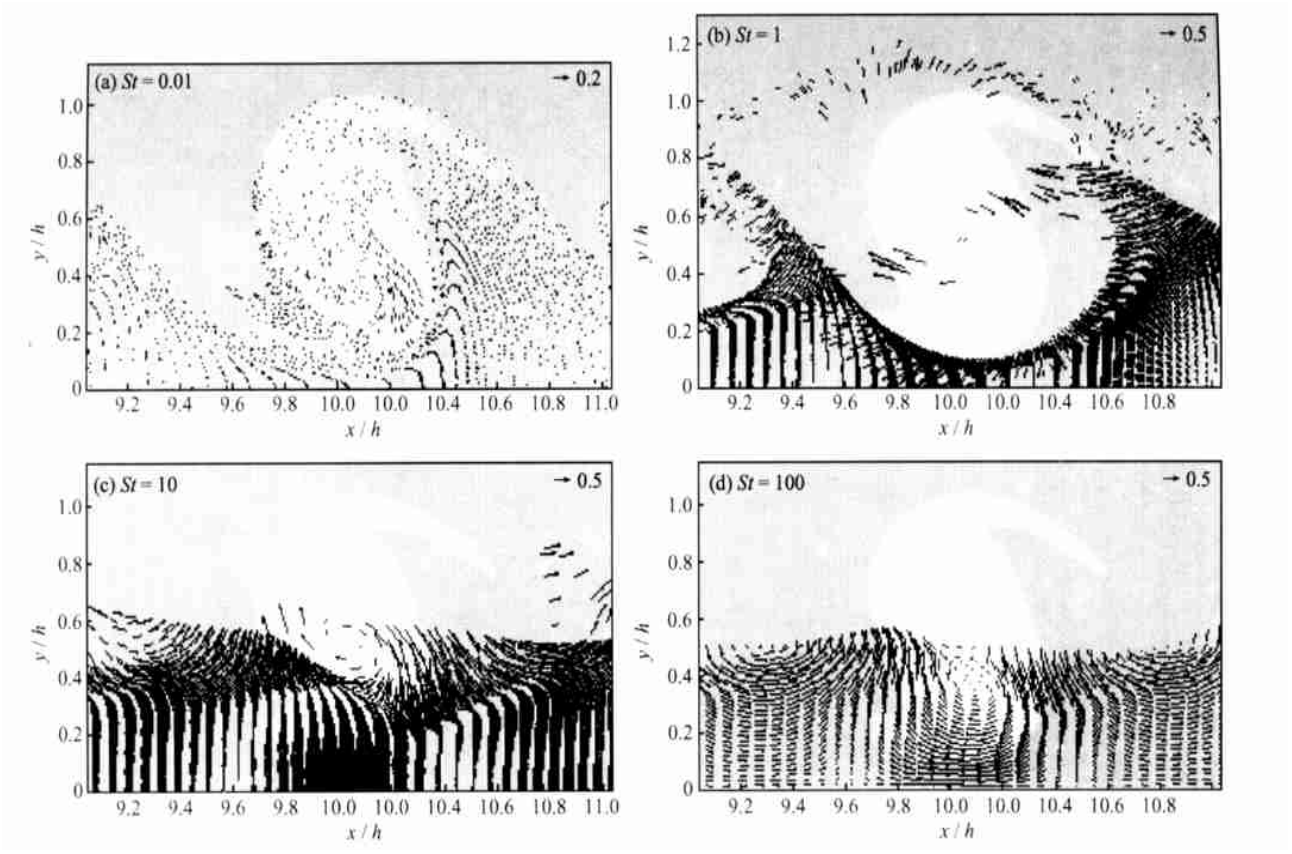

Fig. 8. The relative velocity vector field V_r of particle to the gas phase.

rolling-up and pairing processes, the marching velocities of the flow structures correspond to the convective velocity U_c. The spanwise vortex generally rolls up at $x/h=2.5\sim3$. The biggest lateral widths of 2-pairing and 3-mixing vortexes extend 2 and 3 times that of one spanwise vortex, respectively.

The longitudinal velocity (U) gets to the self-similar state at $x/h=11.5$, and the mean profiles (U) compare well with experimental results, which validates that even 2-dimensional DNS results can represent the 1st-order statistical quantities of "real" flows. Due to the special symmetrical vorticity field, the centerline longitudinal intensities $\sqrt{\overline{u_C^2}}$ grow monotonously until equaling the peak stresses at the shear layer locations, while the lateral intensities $\sqrt{\overline{v_C^2}}$ are inhibited strongly.

The dispersion characteristics of various representative particles, $St=0.01$, 1, 10 and 100, have been studied in this paper to provide helpful references for engineering applications. Particles whose $St=0.01$ can be treated as "tracking" ones. They are fully controlled by the vortexes and reproduce all the large scale structures at the downstream section. As the dynamic response time of particles is identical with the characteristic time of the fluid flow ($St=1$), particles exhibit interesting self-organized behaviors, i.e. most of them spreading outside the vortex kernels, while a few arranging orderly in "line" modes in the pairing vortexes. Large particles of $St=10$ and 100 are less influenced by the large scale structures.

The grid RMS particle numbers, N_{rms}, and relative velocity fields to the gas phase, V_r, have been used as quantity parameters to further prove the above conclusions. N_{rms} ($St=1$) is always the biggest at different time, which validates that particles in such size disperse most non-uniformly and lots of them aggregate in local domains. In V_r plots, the relative velocities of all the particles of $St=0.01$ are almost zero, which indicate that there almost does not exist slippage between particles and air. For particles of $St=1$ located around the vortex kernels, the instantaneous moving directions of V_r point to outside of the kernels, indicating that they will spread out further. At both sides of the above "line" in the vortexes, the magnitudes of V_r of particles are almost the same, but their directions are opposite, and this

"line" lags behind the actual border of the two vortexes in pairing.

It seems that the particle size at $St \sim O(10^{-2})$ is the most preponderant choice in gas-solid two-phase combustion systems in engineering applications according to the above conclusions.

References

1 Bradbury, L. J. S. et al. The spread of a turbulent jet issuing into a parallel moving airstream. J. Fluid Mech., 1967, 27(2): 381.
2 Everitt, K. W. et al. The development and structure of turbulent plane jets. J. Fluid Mech., 1978, 88(3): 563.
3 Sato, H. The stability and transition of a two-dimensional jet. J. Fluid Mech., 1960, 7(1): 53.
4 Rockwell, D. O. et al. Natural breakdown of planar jets. Trans. ASME: J. Basic Engrg., 1972, 1: 720.
5 Antonia, R. A. et al. On the organized motion of a turbulent plane jet. J. Fluid Mech., 1983, 134: 49.
6 Oler, J. W. et al. A vortex-street model of the flow in the similarity region of a two-dimensional free turbulent jet. J. Fluid Mech., 1982, 123: 523.
7 Dai, Y. et al. Large eddy simulation of plane turbulent jet flow using a new outflow velocity boundary condition. JSME Internat. J., 1994, 37(2): 242.
8 Reichert, R. S. et al. Numerical simulation of compressible plane jets. AIAA paper, 1997, 97~1924.
9 Grinstein, F. F. et al. Near field dynamics of subsonic free square jets. A computational and experimental study. Phys. Fluids, 1995, 7(6): 1483.
10 Grinstein, F. F. et al. Dynamics of coherent structures and transitions to turbulence in free square jets. Phys. Fluids, 1996, 8(5): 1237.
11 Urbin, G. et al. Large eddy simulation of three-dimensional spatially evolving round jets. In: Proceedings Eleventh Symposium on Turbulent Shear Flows. Grenoble: Springer-Verlag, 1997.
12 Boersma, B. J. et al. A numerical investigation on the effect of the inflow conditions on the self-similar region of a round jet. Phys. Fluids, 1998, 10(4): 899.
13 Chein, R. et al. Simulation of particle dispersion in a two-dimensional mixing layer. AIChE J., 1988, 34: 946.
14 Wen, F. et al. Particle dispersion by vortex structures in plane mixing layers. J. Fluids Engr., 1992, 114: 657.
15 Chung, J. N. et al. Simulation of particle dispersion in an axisymmetric jet. J. Fluid Mech., 1988, 186: 199.
16 Tang, L. et al. Self-organizing particle dispersion mechanism in free shear flows. Phys. Fluids A, 1992, 4: 2244.
17 Tang, L. et al. A numerical model for droplets dispersing in a shear layer including coupling effects. ASME FED, 1990, 91: 27.
18 Fan, J. R. et al. Direct simulation of particle dispersion in a three-dimensional temporal mixing layer. Proc. R. Soc. London A, 2001, 457: 2152.
19 Lele, S. K. Compact finite difference schemes with spectral-like resolution. J. Comput. Phys., 1992, 103: 16.
20 Carpenter, M. H. et al. Fourth-order 2n-storage Runge-Kutta schemes. NASA Technical Memorandum, 1994, TM109112.
21 Thompson, K. W. Time dependent boundary conditions for hyperbolic systems. J. Comput. Phys., 1987, 68: 1.
22 Thompson, K. W. Time-dependent boundary conditions for hyperbolic systems ii. J. Comput. Phys., 1990, 89: 439.
23 Rudy, D. H. et al. A nonreflecting outflow boundary condition for subsonic Navier-Stokes calculations. J. Comput. Phys., 1980, 36: 55.
24 Poinsot, T. J. et al. Boundary conditions for direct simulations of compressible viscous flows. J. Comput. Phys., 1992, 101: 104.
25 Hu, F. Q. On absorbing boundary conditions for linearized Euler equations by a perfectly matched layer. J. Comput. Phys., 1996, 129: 201.
26 Hu, F. Q. A stable, perfectly matched layer for linearized Euler equations in unsplit physical variables. J. Comput. Phys., 2001, 173: 455.
27 Tong, B. G. et al. Unsteady flows and vortex dynamics (in Chinese). Beijing: National Defence Industry Press, 1993.
28 Gutmark, E. et al. The planar turbulent jet. J. Fluid Mech., 1976, 73(3): 465.